Electrons in coupled vertical quantum dots: Interdot tunneling and Coulomb correlation

Garnett W. Bryant
Microphotonic Devices Branch, U.S. Army Research Laboratory, Adelphi, Maryland 20783-1197
(Received 19 March 1993)

Interdot tunneling, lateral confinement, and Coulomb correlation determine how charge is transferred when a bias is applied between the dots in coupled quantum dot systems. The effective-mass Schrödinger equation for interacting electrons confined in coupled vertical double-dot systems is solved to study interdot charge transfer. The configuration-interaction method is used to explicitly include intradot and interdot electron correlation. The energy spectra, charge densities, and correlation functions for interacting two-electron systems in coupled dots are presented as functions of the applied bias between the dots. In small dots with strong lateral confinement, where the Coulomb energies are larger than the interdot tunneling resonances, the total charge on a dot changes in integer jumps as a bias is applied. Lateral correlation is inhibited by strong lateral confinement and charge tunneling out of a dot is uncorrelated to the charge remaining in the dot. The dot charge changes more smoothly with applied bias when the dots are more strongly coupled by interdot tunneling or in larger dots where intradot correlation causes large intradot charge separation, which reduces charging energies and suppresses the Coulomb blockade of charge transfer. In large dots, charge tunneling out of a dot remains strongly correlated to charge left on the dot. To study charging in vertical quantum dot resonant-tunneling structures, the dots must be wide enough that charging energies are large compared to the single-particle-level spacings, but not so large that intradot correlation strongly suppresses the charging energies and Coulomb blockade effects.

I. INTRODUCTION

Resonant tunneling spectroscopy has been used extensively in recent years to probe electron states in zero-dimensional vertical quantum dot structures.[1–17] The vertical quantum dot structures are fabricated from two-dimensional resonant-tunneling structures by confining lateral motion in the contact regions, the barriers, and the wells (as shown in Fig. 1). The laterally confined contacts are the quantum wires that connect to the quantum dots. Fine structure superimposed on a two-dimensional resonant-tunnelinglike current-voltage characteristic has been observed[1–17] for resonant tunneling through small dots.

Two effects contribute to the observed fine structure. When the barriers connecting the dots to the emitter and collector are thin, charge that tunnels onto the dots will tunnel off the dot before additional charge tunnels on. In that case, the transport is a single-particle process. Steplike jumps in the single-particle resonant-tunneling current-voltage characteristic occur when dot states which can couple by tunneling to the occupied emitter states are resonant with the emitter Fermi level.[18,19] The single-particle-level splitting in the dot determines the spacing of fine-structure peaks in the current-voltage characteristic. Resonant tunneling should, in principle, provide a quantitative spectroscopy of confined states in these quantum dots.

When the barriers connecting the dots to the emitter and collector are thick, charge can be trapped on the dots long enough to impede transport of additional charge through the quantum dots (Coulomb blockade). When charging effects are important,[20–22] the spacing of fine-structure peaks is determined by the charging energy needed to place an additional charge on the dot as well as the single-particle-level splitting in the dot. In very large dots (such as Coulomb islands formed by lateral gating of two-dimensional electron gases), the charging energy can be much larger than the single-particle-level splitting and the spacing of fine-structure peaks is determined mainly by the charging energy. In vertical quantum dot struc-

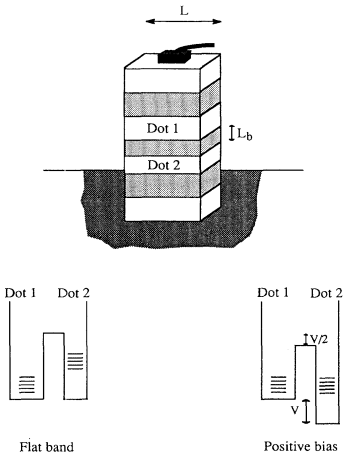

FIG. 1. Schematic of a vertical quantum dot resonant-tunneling structure. A coupled-dot structure with lateral dimension L is shown. The two dots are coupled through a barrier of width L_b. The potentials used to model the conduction-band profile along the growth direction of the quantum-well system are shown for flatband and for applied bias V. The levels indicate the lowest well subband quantized by lateral confinement.

0163-1829/93/48(11)/8024(11)/$06.00

tures, the charging energies and the single-particle-level splittings are comparable. Clear identification of the effects of charging and of single-particle resonant tunneling in vertical quantum dot structures require that one know which quantum dot structures can trap charge long enough to cause Coulomb blockade and how big charging energies are in these structures.

The basic ingredients needed for Coulomb blockade[23] are particle-number quantization on the quantum dot and a charging energy. In that case, the quantum dot exists in integer charge states separated by well-defined energies. Qualitatively, one expects the particle number to be quantized if the charging energy is much greater than the resonance linewidth for tunneling into the dot. If the charging energy can be defined by a capacitance $E_c = e^2/2C$ and the tunneling time by an RC time constant, then the resonance linewidth is much less than the charging energy when $1/R \ll 2e^2/h$, the conductance of a channel with a transmission coefficient of one. The transmission coefficient at resonance for tunneling though a state in a double-barrier resonant-tunneling structure is one when each barrier has the same transmission coefficient. Incomplete transmission occurs when one barrier is more transmitting than the other barrier. Thus, particle-number quantization on the dot should occur when one barrier is much thicker than the other barrier. Intuitively, the barrier connecting the dot to the collector should be the thick barrier and the barrier connecting the dot to the emitter should be the thin barrier so that charge can tunnel easily from the emitter to the dot and tunnel slowly to the collector. A wide variety of vertical quantum dot structures have been studied.[1–17] Structures with symmetric barriers and with asymmetric barriers have been probed. The well widths range from 4 to 10 nm, barrier widths from 5 to 14 nm, barrier heights from 100 to 300 meV, and lateral sizes from 50 to 500 nm. It is important to know which structures should display charging effects.

In this paper, interacting two-electron systems confined in coupled quantum dot structures are studied to better understand the interplay of lateral confinement, interdot tunneling, and intradot and interdot Coulomb correlation when all of these effects are important.[24] The coupled quantum dot structures considered are vertical, coupled, double-dot structures, formed by lateral confinement of coupled double quantum wells (as shown in Fig. 1). The lateral size of vertical quantum dots are typically an order of magnitude larger than the well widths. Lateral Coulomb correlation must be included to properly account for Coulomb effects in these tunneling structures. The calculations presented here explicitly include the effects of lateral Coulomb correlations. The two-electron effective-mass Schrödinger equation for interacting electrons is solved. The configuration-interaction method is used to include electron correlation. This method was used by the author[25] and has been used extensively by others[26–29] to study few-electron systems in isolated dots. Recently, Lent[30] studied the effects of interdot tunneling and Coulomb correlation on two-electron states in a one-dimensional coupled double-dot system. Guerrero[31] used a Hartree-Fock approach to study the influence of the electron-electron interaction on the transfer of charge between quantum dots. Fong *et al.*[32] used a density-functional approach to study the charge distribution during resonant tunneling between coupled dots. None of these approaches[30–32] include the effects of lateral Coulomb correlation.

The model and theory used to study isolated dots[25] is briefly reviewed and the extensions of this model and theory needed to study coupled dots are described in Sec. II. Results are presented in Sec. III. Calculations are done for $GaAs/Al_xGa_{1-x}As$ quantum dot structures with typical barrier widths, barrier heights, and well widths to model realistic structures. The energy spectra, charge densities, and correlation functions for interacting two-electron systems in the coupled dots are presented as a function of the applied bias between the dots. Charging energies are determined from the energy spectra and presented as a function of dot size. Structures with lateral sizes ranging from 20 to 500 nm are studied. In small dots (smaller than 50-nm wide), intradot lateral Coulomb correlation is inhibited by the strong lateral quantization. In large dots (wider than 100 nm), charging energies are substantially reduced and Coulomb blockade effects are significantly suppressed by including the lateral correlations. In large dots, the charge distribution clearly exhibits the lateral correlations between the electrons. When the applied bias brings dot states near resonance, the lateral correlations determine how the charge tunnels between the dots. When lateral correlation is weak and blockade effects are important, the charge tunnels one by one. The first charge to tunnel between the dots is very weakly correlated to the charge remaining in the other dot. When lateral correlation is important, the lateral correlations are preserved as the charge tunnels between the dots. Conclusions are presented in Sec. IV.

II. MODEL AND THEORY

In this paper, the interplay of lateral confinement, Coulomb correlation, and interdot tunneling is investigated by considering few-electron systems in coupled vertical quantum dots (as shown in Fig. 1). The double-dot structures are laterally confined, coupled double-well systems. A tunnel barrier couples the two dots. The other barriers prevent electrons from leaving the coupled-dot structure. This model defines a closed system. Resonant tunneling occurs in open systems with the dots connected to the particle reservoirs of the emitter and collector. Investigating the interplay of tunneling, lateral confinement, and Coulomb correlation in open systems for realistic structures where the Coulomb correlation is treated explicitly without using approximate models, such as the charging model[20–22] used to study Coulomb blockade, would be difficult. Closed systems are studied in this paper so that Coulomb correlation can be fully accounted for.

The model used to study coupled dots[24] is an extension of the model used to study isolated dots.[25] Few-electron systems in isolated systems have been studied by solving the multiparticle effective-mass Schrödinger equation for

interacting electrons in dots modeled as laterally confined, strictly two-dimensional quantum wells. No effects of well width were included. The dots were rectangular, with infinite barriers to provide the lateral confinement. The particle interaction was the Coulomb interaction screened by the background dielectric constant. The correlations were included by the use of a configuration-interaction approach. The multiparticle wave functions were expanded in terms of Slater determinants constructed from the single-particle, particle-in-a-box eigenstates. For the infinite barrier model, a basis set of wave functions separable in the two lateral directions (x and y) that defined the dot was used. The kinetic energy and interaction matrix elements were found by use of the Slater-determinant basis. The Hamiltonian was diagonalized to find the eigenstates of the interacting systems.

For example, for two electrons in an isolated, strictly two-dimensional, square quantum-dot with infinite confining barriers and width L, the Hamiltonian is

$$H = H_{\rm ke} + H_{\rm conf} + H_{\rm int} ,$$

$$H_{\rm ke} = \sum_{i=1,2} \frac{p_{ix}^2 + p_{iy}^2}{2m_e} ,$$

with

$$H_{\rm conf} = \begin{cases} 0, & -L/2 \le x_i, y_i \le L/2, i = 1,2 \\ \infty, & \text{otherwise} , \end{cases}$$

and

$$H_{\rm int} = \frac{e^2}{\varepsilon[(x_1 - x_2)^2 + (y_1 - y_2)^2]^{1/2}}$$

for the kinetic energy with an isotropic effective mass m_e, the lateral confinement potential, and the Coulomb interaction screened by the dielectric constant ε.

Energies and wave functions were found by numerically diagonalizing the Hamiltonian matrix. The basis set used for the calculations was the set of two-particle Slater determinants,

$$\Psi_{n_1,s_1,n_2,s_1} = \frac{(\Phi^1_{n_1,s_1}\Phi^2_{n_2,s_2} - \Phi^1_{n_2,s_2}\Phi^2_{n_1,s_1})}{\sqrt{2}} ,$$

constructed from the single-particle states, with index $n \equiv (n_x, n_y)$,

$$\Phi^i_{n,s} = \phi_{n_x}(x_i)\phi_{n_y}(y_i)\sigma^i_s ,$$

that are products of the eigenstates ϕ_n for the single-particle x (y) kinetic energy and lateral confinement potential

$$\phi_n(x) = \sqrt{2/L}\cos\left[\frac{n\pi x}{L}\right] \quad n \text{ odd}$$

$$= \sqrt{2/L}\sin\left[\frac{n\pi x}{L}\right] \quad n \text{ even} ,$$

with energies

$$E_n = \frac{\hbar^2\pi^2 n^2}{2m_e L^2} ,$$

and the spin states σ_s. The Coulomb matrix elements for the basis set of Slater determinants were found by numerical integration. The Coulomb potential was transformed into a representation[33] that allows the four-dimensional integration for the basis set defined above to be reduced analytically to a one-dimensional integration which was done numerically. The extension of these calculations to systems with more than two electrons is straightforward.

The model used for isolated dots is extended in the following manner to study coupled double dots. First, to simplify the calculations, I assume that the two dots and the tunnel barrier have the same lateral confinement, the same effective mass, and the same dielectric constant. In that case, the Hamiltonian for single-particle motion in the lateral (x and y) directions is separable from the Hamiltonian for single-particle motion in the longitudinal (z) direction and the Hamiltonian for the coupled dot system is obtained by adding the Hamiltonian for single-particle tunneling between the dots to the Hamiltonian for an isolated two-dimensional dot and by using a three-dimensional Coulomb potential screened by the uniform dielectric. The Hamiltonian for the coupled double dots $H_{\rm cd}$ is

$$H_{\rm cd} = H_{\rm ke} + H_{\rm conf} + H_{\rm int(3D)} + H_{\rm tun} ,$$

where $H_{\rm ke}$ and $H_{\rm conf}$ are the lateral kinetic energy and confinement potential used for an isolated dot, independent of z because the effective mass and lateral confinement are assumed to be the same in the two wells and the tunnel barrier, and $H_{\rm int(3D)}$ is the Coulomb interaction extended to three dimensions. For two electrons,

$$H_{\rm int(3D)} = \frac{e^2}{\varepsilon[(x_1 - x_2)^2 + (y_1 - y_2)^2 + (z_1 - z_2)^2]^{1/2}} .$$

$H_{\rm tun}$ is the Hamiltonian for tunneling between the two wells. For two electrons,

$$H_{\rm tun} = \sum_{i=1,2}\left[\frac{p_{iz}^2}{2m_e} + V_i\right] ,$$

where V_i is the conduction-band profile along z that defines the double-well potential. The model used for V_i is described below.

In the calculations for isolated dots, the dots were modeled as strictly two-dimensional, with no thickness. In the model used here for coupled-dot systems, each dot is square with lateral dimension L and a finite well thickness, as shown in Fig. 1. At zero applied bias the one-dimensional (1D) confinement potential V_i of the two coupled wells is modeled by a band profile with an infinite barrier, the first well, the middle barrier with height determined by the band discontinuity, the second well, and another infinite barrier. A flat-band profile is assumed for each region. For finite applied bias between the two wells, the bands are assumed to remain flat with the first well band edge fixed, the middle barrier height

shifted by half the applied bias, and the second well band edge shifted by the applied bias (as shown in Fig. 1).

Energies and wave functions for multiparticle states of the coupled-dot system are found by numerically diagonalizing the Hamiltonian matrix. Typically, the length L of the lateral confinement is much greater than the widths of the two coupled wells. Both intrawell and interwell correlations are important. States are coupled by interwell tunneling so all configurations for the electrons in the two wells can contribute to the states. Correlations should be different for each configuration of the electrons in the two wells. For these reasons, no assumptions are made in these calculations about the form of the correlations in the wave function. The wave functions are expanded in terms of Slater determinants constructed from the single-particle, noninteracting states of the two dots. For the two-electron calculations, the basis set used for the calculations is the set of two-particle Slater determinants

$$\Psi_{n_1,s_1,n_2,s_2}=\frac{(\Phi^1_{n_1,s_2}\Phi^2_{n_2,s_2}-\Phi^1_{n_2,s_2}\Phi^2_{n_1,s_1})}{\sqrt{2}} ,$$

constructed from the single-particle states, with index $n\equiv(n_x,n_y,n_z)$,

$$\Phi^i_{n,s}=\phi_{n_x}(x_i)\phi_{n_y}(y_i)\xi_{n_z}(z_i)\sigma^i_s ,$$

where the ϕ_n's are the eigenstates for the single-particle $x(y)$ kinetic energy and lateral confinement potential for the isolated dot, σ_s is the spin state, and the ξ_n's are the basis states for tunneling between the two dots.

The set of basis states ξ_n are chosen to be states localized either in dot 1 or in dot 2, as indicated in Fig. 2. These basis states are coupled by the interwell tunneling to form the eigenstates of the coupled-well potential. I assume that the two wells are sufficiently narrow that only the lowest-energy single-particle subband in each well can be occupied. In that case I find that two basis states, one state localized in each well, accurately represent the two lowest energy subband states of the coupled double wells when the interwell tunneling couples the basis states. The ξ_n's ($n=1,2$) are chosen to be the single-particle ground states for the potential wells 1 and 2 that are shown in Fig. 2. Potential well 1 (2) is defined by extending the middle barrier of the double-well potential (shown in the upper part of Fig. 2) across well 2 (1) of the double-well profile. The wave functions for these basis states are defined analytically for the piecewise-constant potentials used here. The energies for these basis states are determined numerically to ensure that the basis states vanish at the infinite barriers that define the outer edges of the potential and satisfy the continuity requirements on the state and its derivative at the discontinuity in the potential. The matrix elements for $H_{\rm tun}$ are evaluated analytically by the use of these analytic basis states.

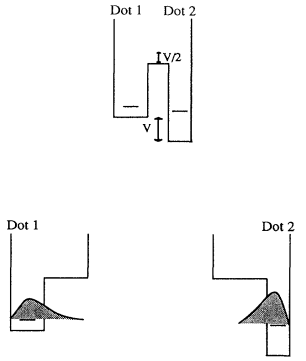

FIG. 2. Basis states used to model the lowest subbands in each well of the coupled-well system. The potential profile of the coupled double well at applied bias V is shown at the top. The potentials used to define the basis states are shown with each basis state.

For the coupled double-dot system, the Coulomb matrix elements are six-dimensional integrals. The integrations over the lateral dimensions are done the same way that the integrals were done for the isolated dots. The six-dimensional integrals for the double-dot systems are reduced analytically to three-dimensional integrals which are done numerically.

Several approximations are used to simplify the calculations. A finite set of basis states is used. Up to six single-particle lateral states for the x motion and for the y motion have been included in the expansion. The Coulomb matrix elements calculated at zero applied bias are used for all biases. Only small changes in the Coulomb matrix elements occur when these matrix elements are recalculated for each applied bias. This approximation is necessary because calculating the Coulomb matrix elements for each applied bias would increase the computer time needed for these calculations by several orders of magnitude. This approximation is accurate because the ξ_n are localized in the wells and do not change much with applied bias. For other sets of the basis functions, such as the actual coupled-well subbands which do change with applied bias, this approximation could not be made. The number of Coulomb matrix elements calculated is further reduced by assuming that all interdot charge-transfer proceeds via single-particle tunneling. No Coulomb scattering of electrons from dot to dot is included. All Coulomb matrix elements that conserve the total charge on each dot are included. Coulomb matrix elements that change the total charge on a dot are much smaller and are ignored.

Calculations are done for GaAs/Al_xGa_{1-x}As dots. The GaAs effective mass and dielectric constant are used for both wells and the tunneling barrier. The barrier height is typically 250 meV, corresponding to $Al_{0.3}Ga_{0.7}As$.

III. RESULTS

In this paper, coupled-dot structures made from a wide 15-nm well (dot 1 in Fig. 1) and a narrow 10-nm well (dot 2 in Fig. 1) are discussed. Other structures made from narrower wells have been investigated. The main effect of reducing the well width is to increase the interwell tunneling. Two-electron systems have been studied. Results

are presented as a function of the lateral size L, the width of the tunnel barrier L_b, and the applied bias V between the dots. A particular positive bias applied to dot 2 brings the states in dot 2 into resonance with the states in dot 1. The dots considered in this paper have a square lateral cross section. The two-electron states are characterized by their parity in the two lateral directions (the x and y directions) parallel to the sides of the square.

The ground state in these coupled-dot structures is a spin-unpolarized state (one electron with spin up and one with spin down), with even x and y parity. The first eight energy levels for two-electron states with the ground-state symmetry are shown for noninteracting electrons in Fig. 3 and for interacting electrons in Fig. 4. In both cases, the electrons are confined in a 20-nm-wide double-dot structure coupled by a 3-nm barrier. Both electrons are in dot 1 when the energy levels are independent of bias. Both electrons are in dot 2 when the levels vary linearly with bias with the largest slope. One electron is in each dot when the levels change linearly with bias with intermediate slope. The lowest energy level for each configuration is labeled in Fig. 3. Other levels are for electrons in higher-energy lateral states. The spin-unpolarized states can have total spin $S=0$ or 1. States with both electrons in the same dot are spin-singlet states. States with one electron in each dot can be singlet or triplet states. The degeneracies of the noninteracting states at $V=-50$ meV are indicated in Fig. 3. These degeneracies change as the bias is varied. For noninteracting electrons, the single-particle resonant tunneling occurs at a bias of 22 meV. Other level crossings are shown in Fig. 3. These correspond to the crossing of states with electrons in different lateral states. No tunneling occurs at these other crossings because lateral-mode mixing is not included in these calculations.

The levels shift to higher energy and the degeneracies

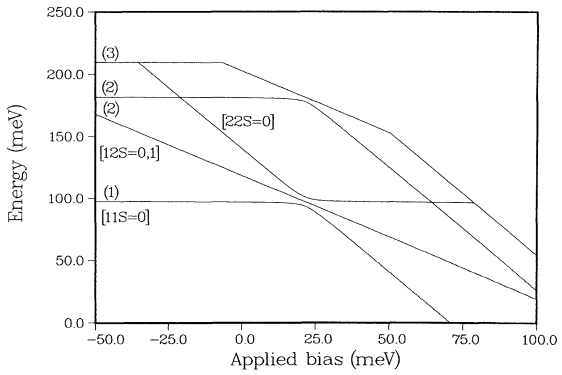

FIG. 3. Energy levels for two noninteracting electrons in spin-unpolarized, even-parity states confined in a coupled double-dot structure made from 15- and 10-nm wells with $L=20$ nm and $L_b=3$ nm. The first eight levels with this symmetry are shown, the degeneracies are indicated in parentheses. The dependence on applied bias is shown. The lowest-energy configurations of the electrons in the two dots are labeled as $[ijS]$ where i and j indicate which dot the electrons are in and S is the total spin. The single-particle resonance occurs at a bias of 22 meV.

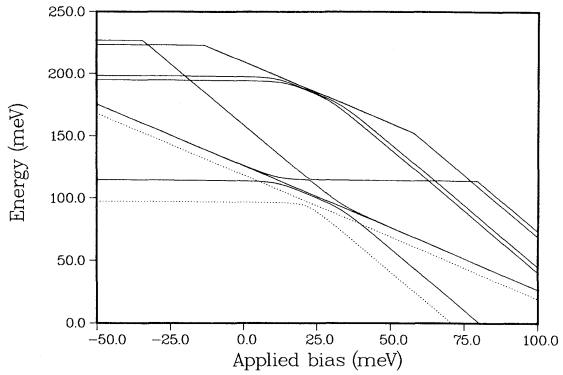

FIG. 4. Energy levels (solid curves) for two interacting electrons in spin-unpolarized, even-parity states confined in a coupled double-dot structure with $L=20$ nm and $L_b=3$ nm. The two lowest-energy levels for noninteracting electrons (see Fig. 3) are shown for comparison (dotted curves). The first eight levels for interacting electrons with this symmetry are shown; comparison with Fig. 3 shows how the degeneracies are lifted by the Coulomb interaction.

are split due to the electron-electron repulsion (see Fig. 4). The energy increase is larger for states with both electrons in the same dot than for states with one electron in each dot. The lowest-energy configuration with one electron in each dot is doubly degenerate when the electrons are noninteracting. When interactions are included, this degeneracy is lifted near the resonance. The triplet state with one electron in each dot cannot couple to the singlet states with both electrons in either dot 1 or dot 2. However, electrons can tunnel between the dots by the coupling of the singlet state for one electron in each dot with the singlet states for both electrons in the same dot. Care must be taken in identifying the resonances that participate in the charge transfer between the dots. Charge transfer between the dots occurs when the applied bias brings into resonance two states with different dot charge that are mixed by the single-particle tunneling or the Coulomb interaction. Coulomb mixing of states with different dot charge is not always possible if the state symmetries are different.

The single-particle resonance is split into three resonances. Expulsion of one electron from the ground state with both electrons in dot 1 occurs at a bias before the single-particle resonance. Coulomb blockade prevents the transfer of the second electron to dot 2 until the bias is greater than the single-particle resonance. At the single-particle resonance, a very narrow resonance remains for the simultaneous transfer of two electrons from dot 1 to dot 2. This transfer occurs with negligible change in Coulomb energy and so occurs very near the single-particle resonance.

A key requirement of the orthodox theory of Coulomb blockade of electron transport through quantum dots is that the charge on the dot be an integer and that the dot charge change by integer amounts as a bias is applied to the dot. For interdot tunneling, the ground state should have a well-defined charge configuration with an integer charge in each dot. Figure 5 shows how the width of the

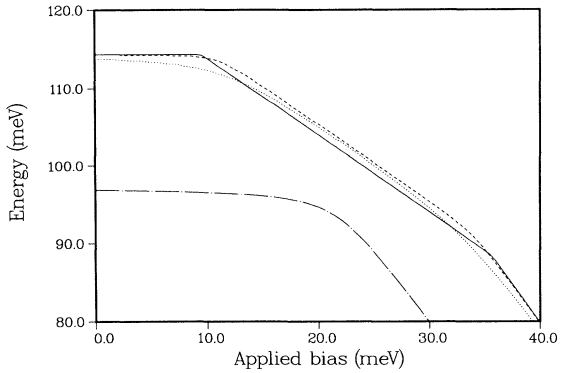

FIG. 5. Ground-state energy of two interacting electrons in a 20-nm-wide structure. Dependence on applied bias for L_b is the following: 3 nm, no Coulomb interaction (dashed-dotted curve); 3 nm (dotted curve); 5 nm (dashed curve); and 10 nm (solid curve).

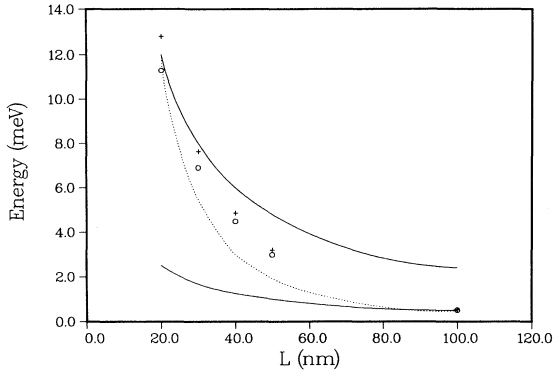

FIG. 6. Charging energy to transfer one electron between dots in a coupled double dot with $L_b=7$ nm. The dependence on L is shown. The circles (pluses) are the charging energies to transfer one electron from the state with one electron in each dot to the state with both electrons dot 1(2). The solid (dotted) curves indicate a $1/L$ ($1/L^2$) dependence on L.

middle barrier effects the configuration of the ground state and the ground-state energy. For thick barriers the resonance width is much less than the Coulomb energies, and the ground state clearly changes from a configuration with two electrons in dot 1, to a configuration with one electron in each dot, then to a configuration with both electrons in dot 2 as the applied bias is increased. The sharpness of the transitions between configurations is blurred for thinner barriers with broader single-particle resonances.

Charging energies can be defined for structures with states that have integer charges in each dot. Consider the case shown in Fig. 4. For the lowest-energy state of each of the three configurations of the two electrons in the two dots, the energy difference between the state found with and without the Coulomb interactions (the difference between the solid and dashed curves in Fig. 4) is constant except near the resonance. This energy difference defines the Coulomb energy for each configuration. The charging energy is the difference in Coulomb energy between having two electrons on the same dot and one electron on each dot. The charging energies for double dots coupled by a 7-nm barrier are shown in Fig. 6. The energy for putting a second electron on dot 2 is slightly higher than the energy for putting a second charge on dot 1, because dot 1 is wider. The solid curves show a $1/L$ scaling that would occur if increasing the dot size just expanded the charge density without changing the distribution of charge. The charging energy decreases much faster than $1/L$. In small dots, single-particle lateral-level spacings are much larger than the Coulomb energies and the intradot correlations are weak. In large dots these energies are comparable and the intradot correlations become important. As the dot size increases, substantial redistribution of the charge density occurs to correlate the electrons and reduce the Coulomb energies. In large dots the charging energies are an order of magnitude smaller than what would be expected from $1/L$ scaling. A model of charging based on parallel-plate capacitors[20–22] would predict an energy that scales as $1/L^2$, as shown by the dotted curve in Fig. 6. For structures with only a few electrons, this scaling also gives a poor fit to the charging energies.

The ground-state energies for double dots with $L_b=7$ nm and different lateral sizes, corresponding to the points in Fig. 6, are shown in Fig. 7. The ground-state energy for noninteracting electrons shifts vertically to lower energy by the difference in lateral confinement energy as L increases but the resonance position and width are independent of L. The charging energy to put a second electron on dot 1 determines how far the single-particle resonance shifts to lower bias for that transition and the charging energy to put a second electron on dot 2 determines how far the single-particle resonance shifts to higher bias for that transition.

Coulomb effects are different for states with other symmetries. The lowest-energy level for states with odd-x or odd-y parity are shown in Fig. 8. These odd-parity states have higher energy than the ground state of even parity

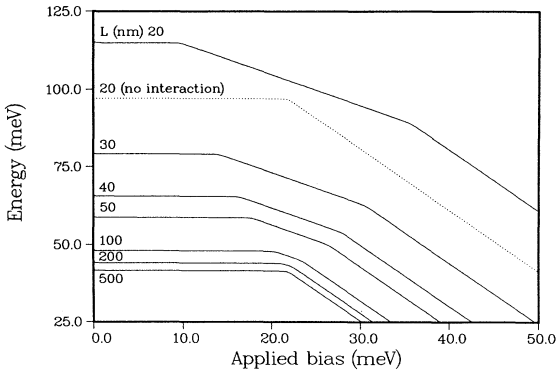

FIG. 7. Ground-state energy of two interacting electrons in a coupled double dot with $L_b=7$ nm. Dependence on applied bias for L is the following: 20 nm (upper solid curve); 20 nm, no Coulomb interaction (dotted curve); 30 nm; 40 nm; 50 nm; 100 nm; 200 nm; and 500 nm.

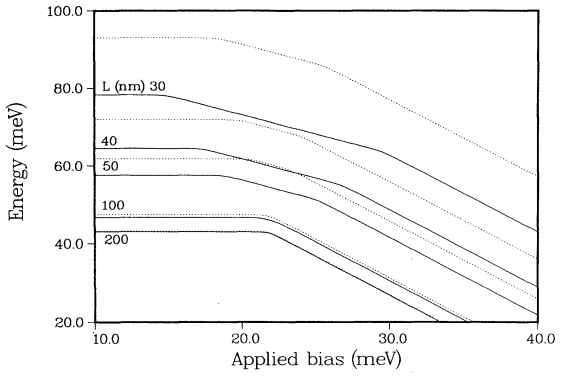

FIG. 8. Comparison of the two-electron energy for the lowest-energy spin-unpolarized, even-parity state (solid curves) with the lowest energy for two-electron states with odd-x or -y parity (dotted curves) for the structure with $L_b=7$ nm. The spin-unpolarized, even-parity state always is the ground state. Dependence on applied bias for L is the following: 30, 40, 50, 100, and 200 nm.

for the same L because excited lateral states are occupied. The Coulomb and charging energies are smaller for the odd-parity states because the electrons are spread further apart in these states. Blockade effects are weaker for these odd-parity states.

The total charge on dot 1 in the ground state is shown in Fig. 9 as a function of applied bias and barrier width for $L=20$ nm. These dots have large Coulomb energies. For noninteracting electrons, the charge changes continuously from two to zero as the bias is tuned through resonance. When the interactions are included, a plateau of unit charge develops around the resonance as a result of the Coulomb expulsion below resonance and the Coulomb blockade above resonance. This plateau becomes flatter and sharper, reflecting discrete, integer charge transfer, as L_b increases. To observe Coulomb blockade in double-dot structures, care must be taken to use barriers thick enough ($L_b=7$ nm, in this case) to produce plateaus. Tunneling depends exponentially on barrier thickness, so small changes in barrier thickness make large changes in the sharpness of the plateaus.

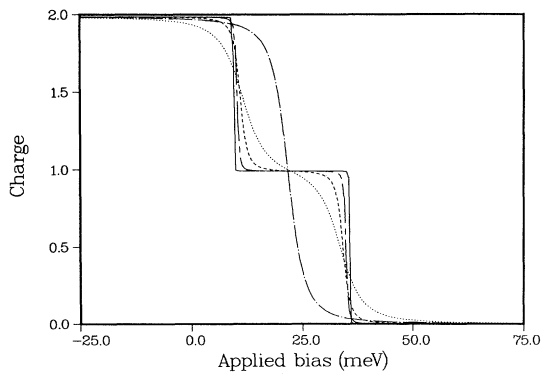

FIG. 9. Total charge on dot 1 for the ground state of two interacting electrons in a coupled double dot with $L=20$ nm. Dependence on applied bias for L_b is the following: 3 nm, no Coulomb interaction (dashed-dotted curve); 3 nm (dotted): 5 nm (dashed); 7 nm (long-short dashed); and 10 mm (solid). Charge measured in units of the electron charge.

Coulomb energies decrease and the plateaus become narrower when L increases (see Fig. 10). For double dots with $L_b=7$ nm, the plateau is absent for $L=100$ nm. For $L_b=10$ nm, the plateau is present in 100-nm-wide dots but not in 200-nm-wide dots. Calculations have been done to exclude the effects of lateral correlation by allowing the electrons to only occupy the lowest lateral state in each dot (dotted curves in Fig. 10). In wide dots, substantial intradot correlation occurs and intradot charge separation is large enough to suppress the Coulomb blockade. Lateral correlation must be included to accurately model charging effects.

Intradot and interdot correlation influence how the charge is distributed within the dots and how the charge is spread between the dots. First, consider a double-dot structure ($L=50$ nm and $L_b=7$ nm) where intradot correlation is weak and the total charge on each dot has a well-defined one-electron plateau (see Fig. 10). For this structure, dot 1 has two electrons for $V<16$ meV, no electrons for $V>26$ meV, and one electron for 20 meV $<V<24$ meV. The charge density in dot 1 at the center of the dot along the diagonal out to a corner is shown in Fig. 11. Intradot correlations are weak so the density exhibits the distribution expected for electrons in the lowest-energy lateral states. The charge density clearly exhibits the integer jumps in total charge as the bias is changed. The conditional charge density at the center of dot 1 along the diagonal when one electron is at the center of dot 1 is shown in Fig. 12. The charge is weakly correlated to stay away from the other electron at the center of dot 1. The conditional charge density is negligible for $V>20$ meV when the total charge on dot 1 is no more than one electron. The conditional charge

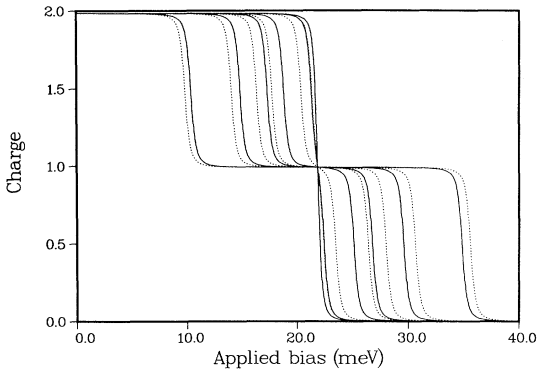

FIG. 10. Total charge on dot 1 (in units of the electron charge) for the ground state of two interacting electrons in a coupled double dot with $L_b=7$ nm. Dependence on applied bias for L is the following: 20, 30, 40, 50, 100, and 500 nm. The plateaus at unit charge decrease with increasing L (each curve is nearly symmetric about the crossover). Solid curves include the effects of intradot correlations. The dotted curves are obtained including only the lowest lateral state and allow no intradot correlation.

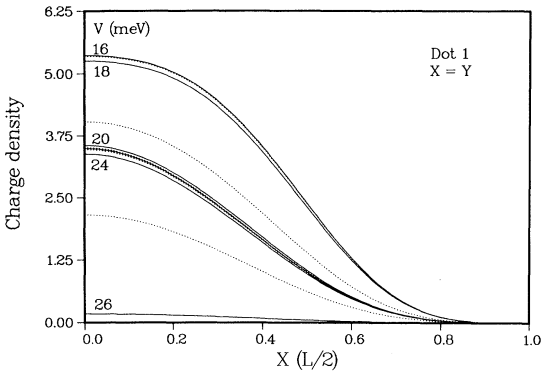

FIG. 11. Ground-state charge density (in arbitrary units) of a coupled-dot structure ($L=50$ nm and $L_b=7$ nm) at the center of dot 1 along the diagonal from the center of the dot to the corner for applied bias from 16 to 26 meV (solid and dashed curves alternate in 1-meV increments).

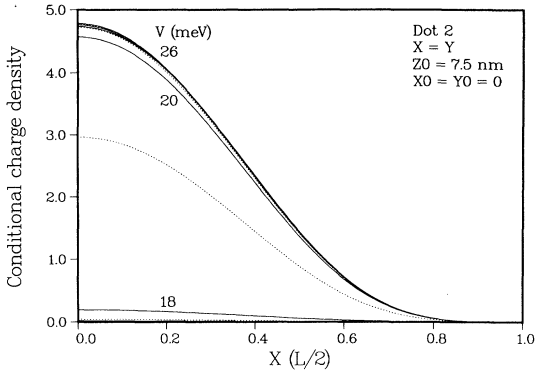

FIG. 13. Conditional charge density of a coupled-dot structure ($L=50$ nm and $L_b=7$ nm) at the center of dot 2 along a diagonal when the other electron is at the center of dot 1 for applied bias from 17 to 26 meV (solid and dashed curves alternate in 1-meV increments). The conditional charge density is negligible for $V<17$ meV.

density at the center of dot 2 along the diagonal, when the other electron is at the center of dot 1, is shown in Fig. 13. The charge on dot 2 is nearly uncorrelated to the charge on dot 1 when lateral correlations are weak. The peak in the conditional charge density on dot 2 is always at the dot center. At large x, the conditional charge density on dot 2 increases monotonically with increasing bias. However, the conditional charge density at the center of dot 2 first increases with increasing bias, reaches a maximum, and then decreases slightly with increasing bias. This behavior is difficult to see in Fig. 13. This variation is much clearer in structures where intradot correlation is more important.

Next, consider a double-dot structure ($L=100$ nm and $L_b=7$ nm) where intradot correlation is strong enough to suppress the one-electron plateau in the total charge (see Fig. 10). The charge density in dot 1 at the center of the dot along the diagonal is shown in Fig. 14. The density exhibits intradot correlation with the peak charge density away from the dot center when the dot has more than one electron. Weak correlations still persist when the dot has less than one charge, although the peak has moved back to the dot center, because the distribution is broader than a single-particle distribution. The charge density no longer clearly exhibits integer jumps in total charge as the bias is changed. The conditional charge density at the center of dot 1 along the diagonal when the other electron is at the center of dot 1 is shown in Fig. 15. The charge is strongly correlated to stay away from the electron at the center of dot 1. This correlation persists as the electron tunnels out of dot 1. The conditional charge density at the center of dot 2 along the diagonal, when the other electron is at the center of dot 1, is shown in Fig. 16. The charge on dot 2 is correlated to the electron on dot 1 when lateral correlations are important. The peak conditional charge density on dot 2 is away from the dot center. At large x, the conditional charge density on dot 2 still increases monotonically with increasing bias. However, the conditional charge density at the center of dot 2 clearly first increases with increasing bias,

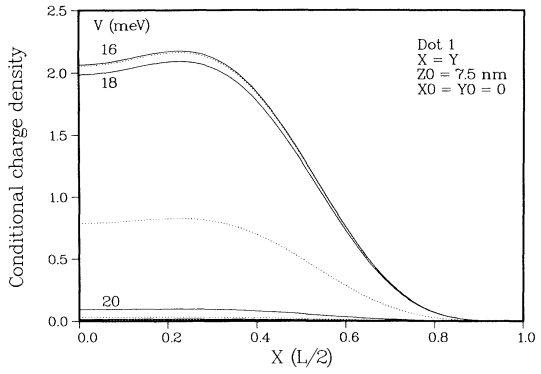

FIG. 12. Conditional charge density of a coupled-dot structure ($L=50$ nm and $L_b=7$ nm) at the center of dot 1 along a diagonal when the other electron is at (x_0,y_0,z_0), the center of dot 1, for applied bias from 16 to 22 meV (solid and dashed curves alternate in 1-meV increments). The conditional charge density is negligible for $V>22$ meV.

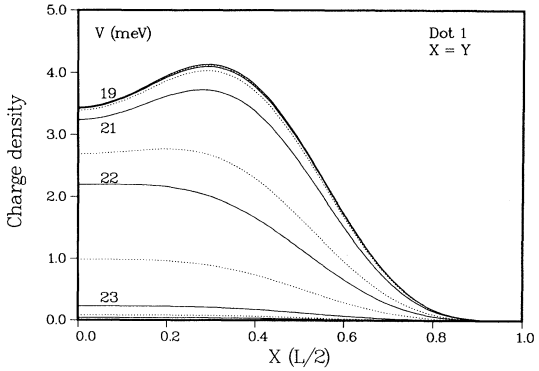

FIG. 14. Ground-state charge density of a coupled-dot structure ($L=100$ nm and $L_b=7$ nm) at the center of dot 1 along a diagonal for applied bias from 19 to 24 meV (solid and dashed curves alternate in 0.5-meV increments).

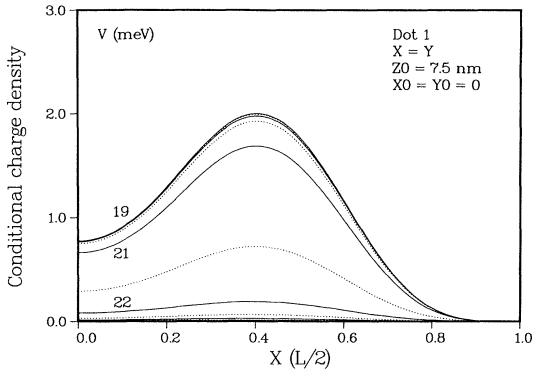

FIG. 15. Conditional charge density of a coupled-dot structure ($L=100$ nm and $L_b=7$ nm) at the center of dot 1 along a diagonal when the other electron is at the center of dot 1 for applied bias from 19 to 23 meV (solid and dashed curves alternate in 0.5-meV increments). The conditional charge density is negligible for $V>23$ meV.

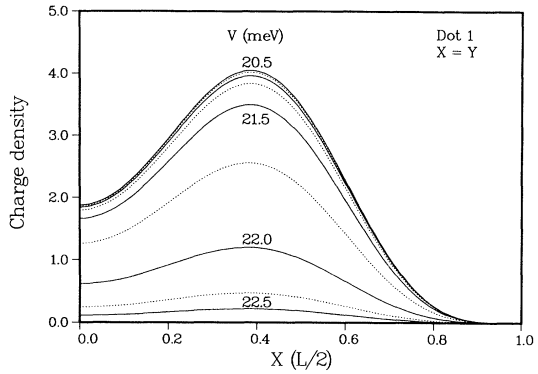

FIG. 17. Ground-state charge density of a coupled-dot structure ($L=200$ nm and $L_b=7$ nm) at the center of dot 1 along a diagonal for applied bias from 20.5 to 22.5 meV (solid and dashed curves alternate in 0.25-meV increments).

reaches a maximum, and then decreases with increasing bias when a full charge has tunneled to dot 2. The charge density and conditional charge density on dot 1 for a case with much stronger intradot correlation (for $L_b=7$ nm and L increased to 200 nm) is shown in Figs. 17 and 18. The conditional charge density on dot 2 for one electron fixed at the center of dot 1 is very similar to the conditional density on dot 1 shown in Fig. 18 (except that the density on dot 2 increases with increasing bias, while the density on dot 1 decreases with increasing bias). The lateral correlations persist even after the charge has tunneled.

The one-electron plateau in the total charge is well defined when $L=100$ nm if L_b is increased to 10 nm. The charge density on dot 1 in this case is shown in Fig. 19. The charge density exhibits the integer jumps in total charge as the bias is changed. However, in this case the intradot correlations clearly remain important when the dot has two charges. The peak charge density is pushed

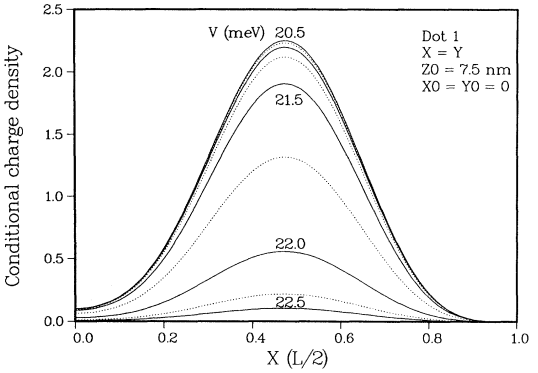

FIG. 18. Conditional charge density of a coupled-dot structure ($L=200$ nm and $L_b=7$ nm) at the center of dot 1 along a diagonal when the other electron is at the center of dot 1 for applied bias from 20.5 to 22.5 meV (solid and dashed curves alternate in 0.25-meV increments).

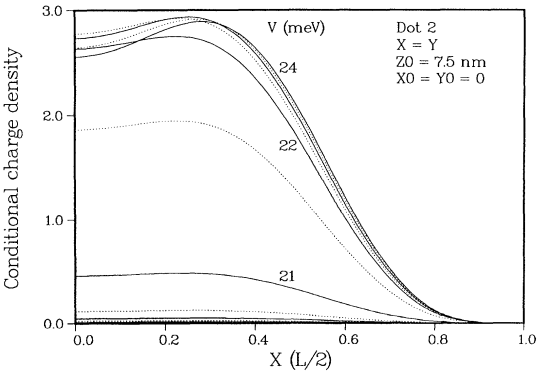

FIG. 16. Conditional charge density of a coupled-dot structure ($L=100$ nm and $L_b=7$ nm) at the center of dot 2 along a diagonal when the other electron is at the center of dot 2 for applied bias from 19 to 24 meV (solid and dashed curves alternate in 0.5-meV increments).

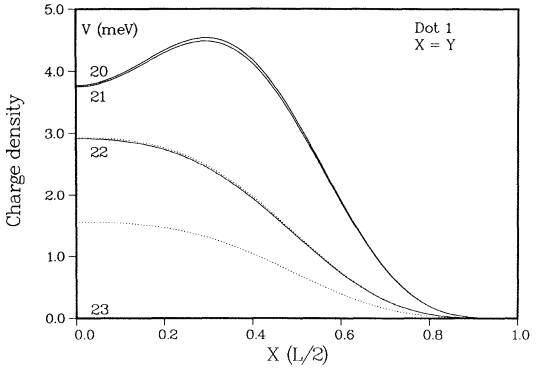

FIG. 19. Ground-state charge density of a coupled-dot structure ($L=100$ nm and $L_b=10$ nm) at the center of dot 1 along a diagonal for applied bias from 20 to 23 meV (solid and dashed curves alternate in 0.5-meV increments).

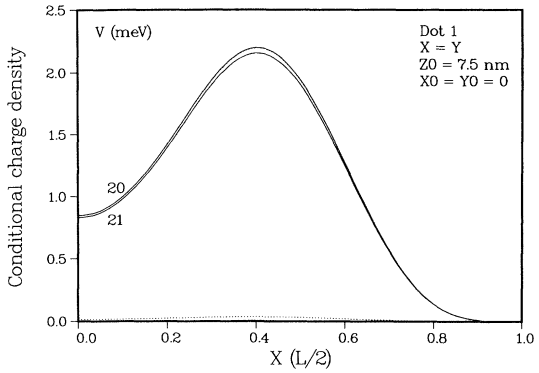

FIG. 20. Conditional charge density of a coupled-dot structure ($L = 100$ nm and $L_b = 10$ nm) at the center of dot 1 along a diagonal when the other electron is at the center of dot 1 for applied bias from 20 to 21.5 meV (solid and dashed curves alternate in 0.5-meV increments). The conditional charge density is negligible for $V > 21.5$ meV.

away from the center when dot 1 has two electrons. The conditional density on dot 1 also shows strong intradot correlation (see Fig. 20). The conditional charge density on dot 2 is also correlated to the charge remaining on dot 1, with a peak away from the center of the dot and nonmonotonic variation in the conditional charge density with increasing bias similar to the variation shown in Fig. 16.

IV. CONCLUSIONS

In coupled vertical double-dot systems, interdot tunneling, lateral confinement, and intradot correlation determine how charge transfers between the dots and whether the dot charge changes in integer jumps as a bias is applied. In small dots with strong lateral confinement, where the Coulomb energies are larger than the interdot tunneling resonance widths, the charge changes in integral jumps. The charge changes more smoothly with applied bias when the dots are more strongly coupled by interdot tunneling or in larger dots where intradot correlation causes large intradot charge separation, which reduces the Coulomb repulsion by an order of magnitude and suppresses the Coulomb blockade. In small dots, lateral correlation is inhibited by strong lateral confinement and charge tunneling out of a dot is uncorrelated to charge remaining in the dot. In large dots, charge tunneling out of a dot remains strongly correlated to charge left on the dot.

Tunnel resonances depend exponentially on barrier thickness. Great care must be taken in choosing vertical quantum dot resonant-tunneling structures to study charging to ensure that the barriers are thick enough to effectively trap charge. Care must be taken in choosing the dot size. The dots should be wide enough that charging energies are large compared to the single-particle level spacings. However, if the dots are too large, then intradot correlation strongly suppresses the charging energies and the interdot tunneling resonance broadens away the integer charge plateaus in the total dot charge. Recent resonant-tunneling experiments on vertical quantum dots with thick asymmetric barriers[8,11,12] reveal large asymmetries in the current for forward and reverse bias. The asymmetries in the current have been attributed to single-particle tunneling for transport in the direction with the thick barrier coupling the dot to the emitter and to charging for transport in the opposite direction where the thick barrier inhibits tunneling from the dot into the collector. These experiments have been done with large dots ($L = 100$–300 nm). Intradot correlation should strongly suppress charging energies and Coulomb blockade effects in these structures. It is not clear that these structures should exhibit large charging effects, despite the intriguing asymmetries revealed by the resonant-tunneling current.

[1]M. A. Reed, J. N. Randall, R. J. Aggarwal, R. J. Matyi, T. M. Moore, and A. E. Wetsel, Phys. Rev. Lett. **60**, 535 (1988).
[2]M. A. Reed *et al.*, in *Festkorperprobleme: Advances in Solid State Physics,* edited by U. Rössler (Springer, Berlin, 1989), Vol. 29, p. 267.
[3]S. Tarucha, Y. Hirayama, T. Saku, and T. Kimura, Phys. Rev. B **41**, 5459 (1990).
[4]S. Tarucha, Y. Hirayama, and Y. Tokura, Appl. Phys. Lett. **58**, 1623 (1991).
[5]S. Tarucha and Y. Hirayama, Phys. Rev. B **43**, 9373 (1991).
[6]M. Tewordt *et al.*, J. Phys. Condens. Matter **2**, 8969 (1990).
[7]H. Asahi *et al.*, Appl. Phys. Lett. **59**, 803 (1991).
[8]M. Tewordt *et al.*, Phys. Rev. B **45**, 14 407 (1992).
[9]M. Tewordt *et al.*, Phys. Rev. B **46**, 3948 (1992).
[10]B. Su, V. J. Goldman, M. Santos, and M. Shayegan, Appl. Phys. Lett. **58**, 747 (1991).
[11]B. Su, V. J. Goldman, and J. E. Cunningham, Science **255**, 313 (1992).
[12]B. Su, V. J. Goldman, and J. E. Cunningham, Phys. Rev. B **46**, 7644 (1992).
[13]M. W. Dellow *et al.*, Phys. Rev. Lett. **68**, 1754 (1992).
[14]P. H. Beton *et al.*, Appl. Phys. Lett. **60**, 2508 (1992).
[15]P. Gueret, N. Blanc, R. Germann, and H. Rothuizen, Phys. Rev. Lett. **68**, 1896 (1992).
[16]M. Van Hove *et al.*, J. Appl. Phys. **72**, 158 (1992).
[17]A. Ramdane, G. Faini, and H. Launois, Z. Phys. B **85**, 389 (1991).
[18]G. W. Bryant, Phys. Rev. B **39**, 3145 (1989).
[19]G. W. Bryant, Phys. Rev. B **44**, 3782 (1991).
[20]H. Grabert and H. Horner, Z. Phys. B **85**, 317 (1991), and other articles in this issue.
[21]D. V. Averin, A. N. Korotkov, and K. K. Likharev, Phys. Rev. B **44**, 6199 (1991).
[22]C. W. J. Beenakker, Phys. Rev. B **44**, 1646 (1991).
[23]C. Pasquier, U. Meirav, F. I. B. Williams, D. C. Glattli, Y. Jin, and B. Etienne, Phys. Rev. Lett. **70**, 69 (1993).
[24]G. W. Bryant, Physica B **189**, 34 (1993).
[25]G. W. Bryant, Phys. Rev. Lett. **59**, 1140 (1987).
[26]P. A. Maksym and T. Chakraborty, Phys. Rev. Lett. **65**, 108 (1990).

[27]U. Merkt, J. Huser, and M. Wagner, Phys. Rev. B **43**, 7320 (1991).
[28]D. Pfannkucke and R. R. Gerhardts, Phys. Rev. B **44**, 13 132 (1991).
[29]W. Hausler, B. Kramer, and J. Masek, Z. Phys. B **85**, 435 (1991).
[30]C. S. Lent, in *Nanostructures and Mesoscopic Systems,* edited by W. P. Kirk and M. A. Reed (Academic, Boston, 1992), p. 183.
[31]A. H. Guerrero, Semicond. Sci. Technol. **7**, B292 (1992).
[32]C. Y. Fong, J. S. Nelson, L. A. Hemstreet, R. F. Gallup, L. L. Chang, and L. Esaki, Phys. Rev. B **46**, 9538 (1992).
[33]G. W. Bryant, Phys. Rev. B **29**, 6632 (1984).